Differential Capacity-Based Modeling for In-Use Battery Diagnostics, Prognostics, and Quality Assurance

Lauren M. Marzocca and Terrill B. Atwater
U.S. Army RDECOM
Communications, Electronics, Research, Development and Engineering Center
Aberdeen Proving Ground, MD 21005

Abstract: *A reliable diagnostic/prognostic indicator for electrochemical systems would allow for the prediction of cell failures, a function that would improve battery safety, efficiency, and quality assurance. The technique of differential capacity has proven to be a useful tool in the pursuit of this type of diagnostic/prognostic device. The plots resulting from the differential capacity technique provide a "fingerprint" of a battery system that can be tracked throughout its life, and changes in these plots give insight into the future behavior of the system. The results of several cell-level galvanostatic experiments – performed on several different chemistry types – will be discussed with respect to differential capacity. This type of galvanostatic cell data was analyzed in order to develop a differential capacity-based model for use in a diagnostic/prognostic device.*

Keywords: state of health; safety; rechargeable lithium-ion battery

Introduction

Differential capacity tracks an electrochemical system's capacity increase on charge or decrease on discharge as a function of voltage. Plotting differential capacity versus voltage creates a snapshot "fingerprint" of the system that can be tracked throughout the system's life. These fingerprints show how characteristic features of the curve change and give information regarding both the underlying thermodynamics and kinetics of the system. Figure 1 gives a visual comparison between a standard voltage versus time discharge plot and a differential capacity plot generated from the same test data. Monitoring the changes in a system's electrochemical properties through differential capacity can help predict failure. This prognostic capability would be useful in preventing safety incidents while also ensuring that a cell or battery is removed from service only after being used to its fullest extent.

Background

Through the Capability Needs Analysis (CNA) process, the U.S. Army derives a list of specific Warfighter requirements that are not currently being met. These requirements are known as CNA gaps. Two power- and energy-related CNA gaps state that "forces lack ability to accurately monitor and manage power demand and supply processes" and that "forces lack comprehensive, institutional awareness of the impact of energy use on operational effectiveness and need to consider efficient use of energy as a mission enabler"[1]. The development of an effective battery diagnostic/prognostic device directly addresses both of these gaps.

A paper investigating the usefulness of the differential capacity technique as a fingerprinting tool for electrochemical systems was presented at the 44th Power Sources Conference[2]. This paper discussed the establishment of the fingerprinting method and included experiments to determine charge/discharge rates (Figure 2) and voltage integration periods (Figure 3) to optimize data fidelity while maintaining test efficiency. To date, the differential capacity technique has been successfully used to study electrochemical systems of varying chemistries, sizes, configurations.

Differential capacity was initially investigated as a quality assurance tool. Generating the differential capacity curves of two identical cells will yield nearly identical curves; therefore, the technique can be used to indentify inconsistencies in a production environment. The analysis of this quality assurance data revealed the possibility for using differential capacity as a prognostic tool. Any changes made to the components of an electrochemical system (different electrodes, electrolyte, material ratios, etc.), as well as any changes in testing conditions (different rates, temperatures, abusive conditions, etc.), will cause changes in that system's fingerprint. This aspect of the differential capacity technique has inherent predictive capabilities, which could be leveraged in a diagnostic/prognostic device.

Failure Prognosis

Experimental: An experiment was designed to bring out cell failure through high-rate charging. The goal was to monitor changes in the differential capacity curve with each cycle of the test and to observe which characteristic feature(s) of the curve changes as a result of performance degradation. A 3.4 Ah NMC 18650 cell was subjected to a cycle life test with a 2 A constant current charge, a 0.8 A constant current discharge, a voltage range of 2.5-4.4 V, and a voltage integration period of 10 mV. The differential capacity curves were tracked as the cell was cycled (Figures 4-6).

Results: The cell experienced significant voltage fluctuation during cycles 9 and 10 but was able to recover for the latter portion of the test, which was stopped at cycle 17. A differential capacity curve was created for each cycle of the test. The curve progression is shown in Figure

4. The blue curves indicate the cycles before the voltage fluctuation, the green curves indicate the cycles during which the fluctuation occurred, and the red curves indicate the cycles after the fluctuation.

Discussion: Figure 5 shows the charge curves for cycles 2-8 (before the voltage fluctuation), and Figure 6 shows the charge curves for cycles 11-17 (after the voltage fluctuation). The characteristic feature of note for this cell is the second charge peak that appears at approximately 3.8 V. As the cycle number increases, in addition to the expected rightward shift, the second charge peak begins to fade. Immediately after the voltage fluctuation, the peak has disappeared entirely. This experiment shows that, for this chemistry, the second charge peak is an indicator of the cell's overall state of health and can therefore be used to predict cell failure in a prognostic device.

Modeling

Experimental: Once the concept of using the differential capacity curve as an indicator for state of health was established, a method of quantifying changes in the curve had to be developed. The Gaussian curve was used as the basis for the differential capacity model. The first experiment that was modeled featured a representative spinel button cell of approximately 10 mAh that was subjected to a 3.5-4.75 V cycle at a rate of 1 mA. A Gaussian curve was used to model the experimental data manually. The general equation for a Gaussian function is given by $f(x) = ae^{-\frac{(x-b)^2}{2c^2}} + d$. For this particular application, *f(x)* equals the differential capacity at potential *x*. Coefficients *a*, *b*, and *c* are the curve-defining parameters and were adjusted manually until the best fit was achieved. Table 1 shows the relationship of each coefficient to its corresponding peak and details what physical values or processes dictate the coefficient values.

Table 1. Gaussian curve-defining coefficients.

Coefficient	Effect on Curve	Function of…
a	Height	Theoretical capacity
b	Position	Theoretical voltage (impedance, activation energy, polarization)
c	Width	Diffusion

Results and Discussion: The first attempt evaluated the accuracy of a two-curve model to simulate the behavior of the spinel button cell, as shown in Figure 7. This method captured the main features of the experimental data but allowed for significant error in certain areas, namely the flat portions of the curve at low and high voltage and the area between the two peaks. To account for this, a third Gaussian curve was added to the model, as shown in Figure 8.

Figures 9-11 show the differential capacity curves and corresponding three-curve Gaussian models at three points – cycle 10, 80, and 130 – during the cycle life test of the aforementioned spinel button cell. Visual inspection of the experimental data indicates a slight change in several of the characteristic features as cycle number increases, especially from cycle 80 to cycle 130, but if differential capacity curves are to be used in a practical state of health device, these feature changes must be quantified. This can be accomplished by monitoring changes in model curve coefficients *a*, *b*, and *c* throughout the life of the cell.

Figures 12 and 13 show the values of coefficients *a*, *b*, and *c* for each of the three Gaussian curves in the model at 10-cycle intervals from cycle 10-130. The *b* and *c* coefficients, shown in Figure 12, follow fairly constant trends throughout the life of the cell. The *a* coefficients, however, shown in Figure 13, begin straying from their respective trends at cycle 80, and then do so more evidently beginning at cycle 110. Monitoring the changes in the coefficients brings out subtle performance degradation in the cell that might not be noticed with only visual inspection. With further testing of different chemistries, a tolerance can be established for each coefficient, which can then be implemented into a diagnostic/prognostic device.

Figure 14 shows the differential capacity curves and the corresponding three-curve Gaussian models (charge only) for cycles 2-5, 10, and 15 of a silicon anode pouch cell. The success of this model indicates that the three-curve Gaussian model is transferrable to other chemistries and cell types. Additionally, this model data shows that, by breaking the experimental data down into three base Gaussian curves and monitoring how each of these curves change as the cell is cycled, the source of the degradation – in this case, the low charge peak – can be pinpointed. With a more thorough knowledge of the physical relevance of each individual Gaussian curve, the model will allow degradation to be pinpointed to a particular component or chemical process within the cell. This capability would be advantageous for both the research and testing communities, where it could be used to more efficiently target recurring issues with new chemistries and manufacturer cells.

Conclusion

The results of this work show that the differential capacity method enhances the ability to predict cell failure and that differential capacity curves can be accurately modeled using Gaussian curves. This type of model utilizes *a*, *b*, and *c* coefficients to quantify and monitor curve changes, which is important if this technique is to be implemented in an in-use battery diagnostic/prognostic device. Future work will include the investigation of other types of failure modes in order to increase the robustness of the method and obtain the necessary data for device implementation.

The three-curve Gaussian model was able to be transferred to a different chemistry and cell type. In the future, more

chemistries and cell types will be modeled using the three-curve method to determine whether other types of models will need to be explored. It is also important to understand the physical relevance of each of the model curves in order to better identify the precise causes of cell failure.

References

1. DiGiosaffatte, M. "Capability Needs Analysis." *Army Capabilities Integration Center*. http://www.arcic.army.mil/Articles/aid-Capability-Needs-Analysis.aspx.
2. Atwater, T.B., P.C. Tavares, and L.M. Marzocca. *P. 44th Power Sources Conference*, 2010.
3. Wright, R.B., et al. *P. 201st Meeting of the Electrochemical Society*, 2002.
4. Bloom, I., et al. *P. 204th Meeting of the Electrochemical Society*, 2003.

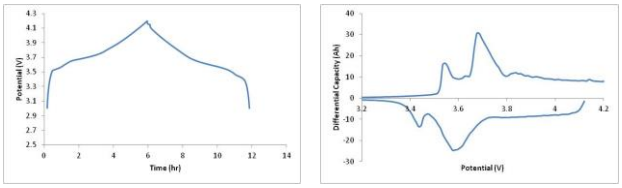

Figure 1. Standard potential vs. time discharge curve compared with corresponding differential capacity curve for a 2.4 Ah NMC 18650 cell.

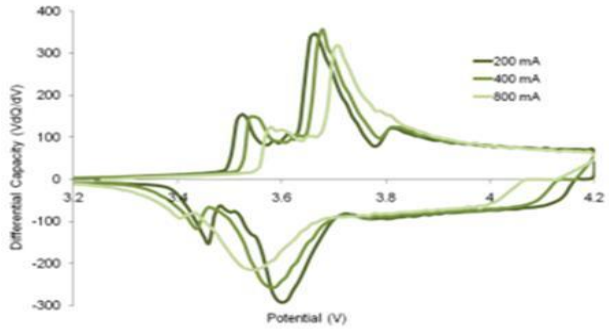

Figure 2. Differential capacity curves comparing data fidelity at varying charge/discharge rates for a 2.4 Ah NMC 18650 cell.

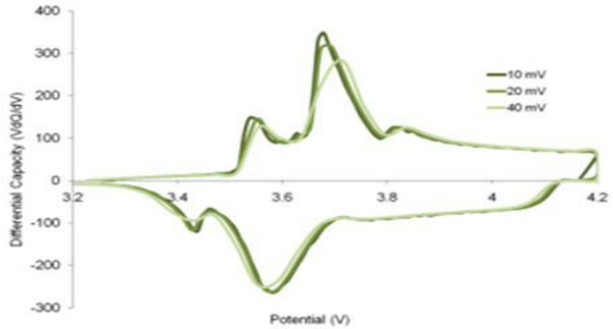

Figure 3. Differential capacity curves comparing data fidelity at varying voltage integration periods for a 2.4 Ah NMC 18650 cell.

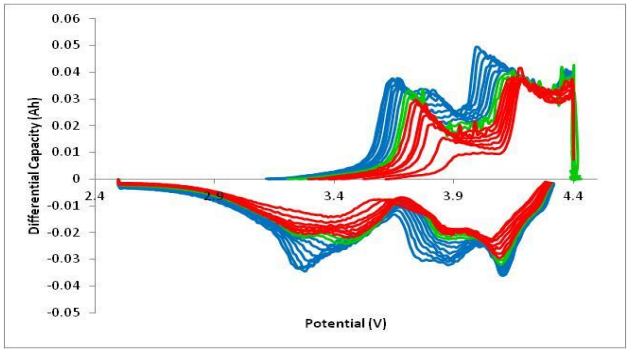

Figure 4. Progression of differential capacity curves during cycle life test for a 3.4 Ah NMC 18650 cell.

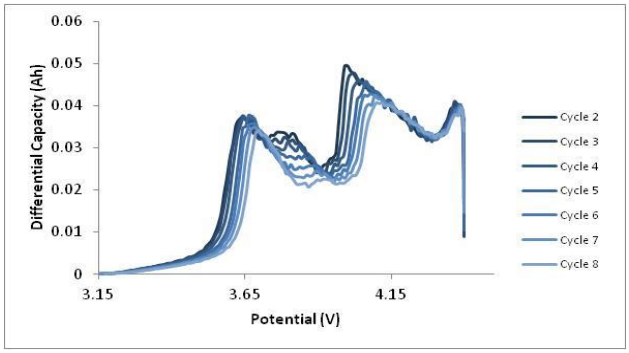

Figure 5. Charge curves before voltage fluctuation for a 3.4 Ah NMC 18650 cell.

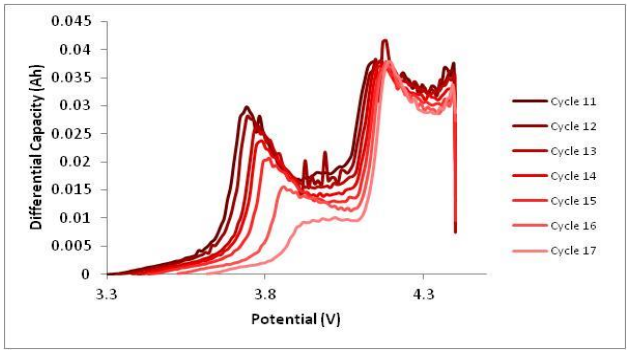

Figure 6. Charge curves after voltage fluctuation for a 3.4 Ah NMC 18650 cell.

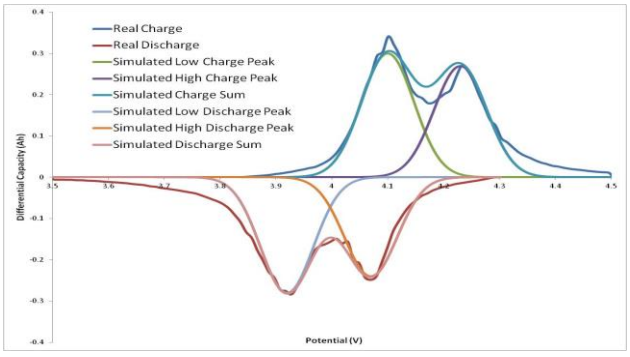

Figure 7. Differential capacity curve with its two-curve Gaussian model for a spinel button cell.

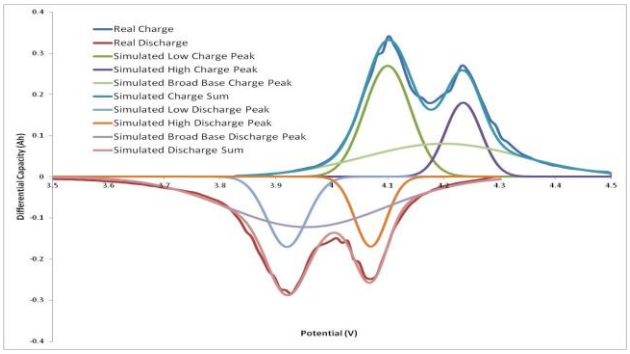

Figure 8. Differential capacity curve with its three-curve Gaussian model for a spinel button cell.

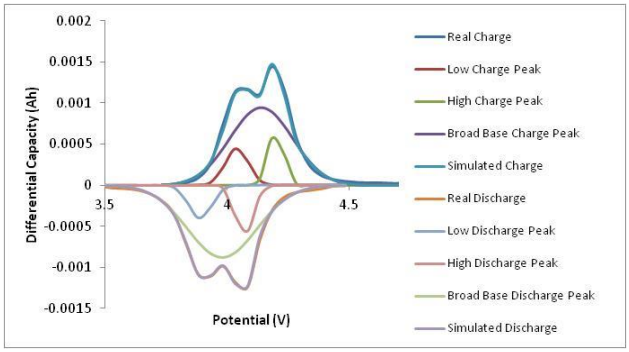

Figure 9. Differential capacity curve with three-curve Gaussian model for a spinel button cell at cycle 10.

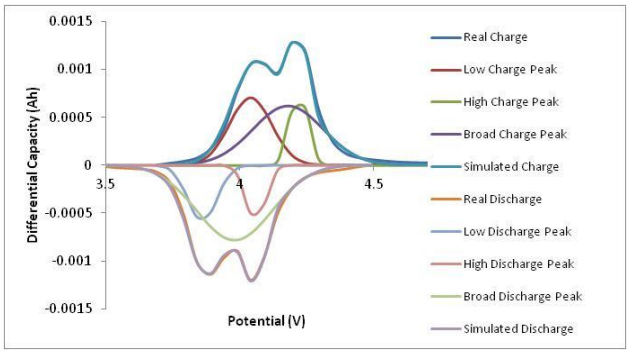

Figure 10. Differential capacity curve with three-curve Gaussian model for a spinel button cell at cycle 80.

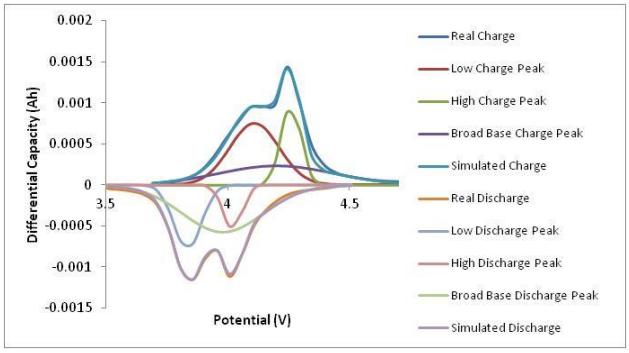

Figure 11. Differential capacity curve with three-curve Gaussian model for a spinel button cell at cycle 130.

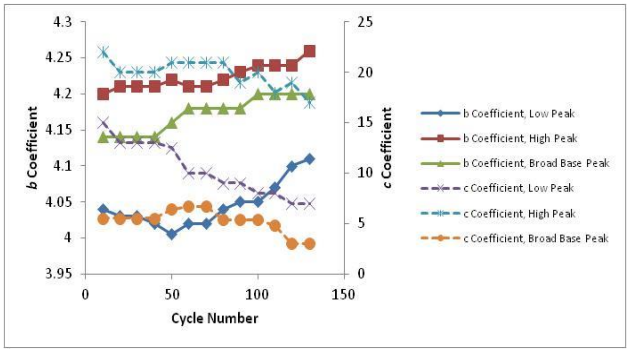

Figure 12. The "*b*" and "*c*" charge coefficients for the three-curve Gaussian model over the life cycle a spinel button cell. The "*b*" coefficients correspond to the primary axis, and the "*c*" coefficients correspond to the secondary axis.

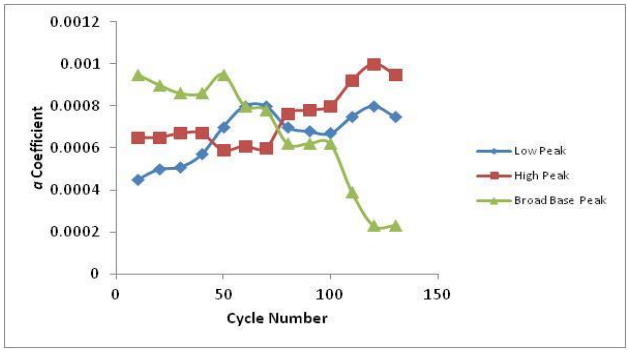

Figure 13. The "*a*" charge coefficients for the three-curve Gaussian model over the life cycle of a spinel button cell.

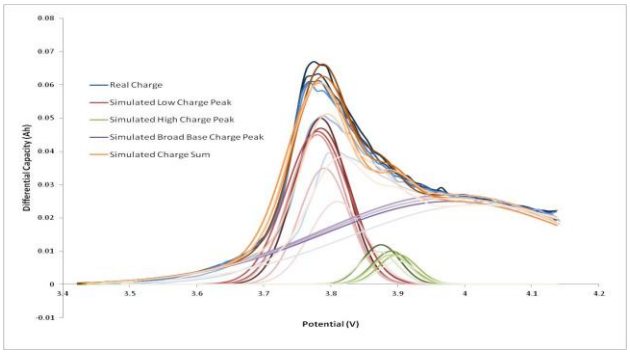

Figure 14. Differential capacity charge curve over the life cycle of a silicon anode pouch cell.